Water Resources Research

TECHNICAL REPORTS: METHODS
10.1029/2018WR023627

The Role of Floodplain Topography in Deriving Basin Discharge Using Passive Microwave Remote Sensing

Seokhyeon Kim[1] **and Ashish Sharma**[1]

[1]School of Civil and Environmental Engineering, University of New South Wales, Sydney, New South Wales, Australia

Key Points:

- The proposed approach uses an automatic thresholding method to refine raw passive microwave remote sensing retrievals for flood detection
- A significant improvement in derived flood signals when compared to discharge observations is noted across 179 diverse basins in Australia
- The proposed method has the potential to improve our ability to detect flood signals in ungauged basins worldwide

Correspondence to:
A. Sharma,
a.sharma@unsw.edu.au

Citation:
Kim, S., & Sharma, A. (2019). The role of floodplain topography in deriving basin discharge using passive microwave remote sensing. *Water Resources Research*, *55*. https://doi.org/10.1029/2018WR023627

Received 4 JUL 2018
Accepted 9 JAN 2019
Accepted article online 17 JAN 2019

Abstract Discharge measurements are essential for a range of hydrologic applications. In situ observations, however, are seldom available. Whereas satellite remote sensing offers a fascinating possibility of deriving discharge data for ungauged catchments, it comes with significant uncertainty and has had limited adoption until recently. A satellite-derived flood signal, referred to as the Measurement-Calibration (MC) ratio, is being increasingly used but suffers from significant uncertainty and inaccuracy, partly because ground geomorphic attributes are ignored in its estimation. We present here an approach for enhancing the MC ratio by accounting for local topography and its impact on flow creation within a catchment. The Topographic Wetness Index is used for extracting the MC ratio from 179 hydrologic reference stations across Australia representing different climates, watershed sizes, and elevations. Results indicate clear improvements in flow estimates using the proposed method as compared to the options currently in place.

1. Introduction

It is typical for hydrologic models to be calibrated using measured discharge at the basin outlet. While in situ observations have been a common source for such discharge data, they are sparsely located in space and only available for limited periods of time. Furthermore, there has been an increasing (and disturbing) tendency to de-commission streamflow gauges and reduce their spatial and temporal coverage across the world according to the Global Runoff Data Centre database (Calmant & Seyler, 2006; Fekete & Vörösmarty, 2002; GRDC/BfG, 2018), making modeling or design even more challenging than before.

As an alternative to in situ discharge data, a satellite-derived flood signal, called Measurement-Calibration (MC) ratio, was initially developed by Brakenridge et al. (2007). The MC ratio is derived from the brightness temperature ratio over wet measurement (M) and dry calibration (C) pixels through various space-borne passive microwave sensors, such as Tropical Rainfall Measuring Mission (TRMM) Microwave Imager (TMI), Advanced Microwave Scanning Radiometer for Earth Observing System (AMSR-E), Advanced Microwave Scanning Radiometer 2 (AMSR2), and Global Precipitation Measurement (GPM) Microwave Imager (GMI). It has been demonstrated that the MC ratio exhibits significant correlations with high discharge values, and hence has been widely tested for use in ungauged basins. Its usage has ranged from calibrating model parameters to estimating river discharge and also monitoring flood peaks and inundation (De Groeve, 2010; Hou et al., 2018; Khan et al., 2012; Revilla-Romero et al., 2015; Tarpanelli et al., 2013; Van Dijk et al., 2016). In addition to this, Revilla-Romero et al. (2014) comprehensively evaluated the product using 322 river measurement locations over the world, and identified dominant factors that influence performance such as upstream area, river width, and vegetation, leading to guidelines on how it should be used in practice.

Despite the potential the MC ratio product exhibits for ungauged basins, there are still open questions as to how one can better isolate discharge for the location of interest from the raw spatially distributed MC ratio data that are collected. It is known that a better signal quality can be obtained when the measurement grid cell is centered over a river reach without regulation by hydraulic structures. Such favorable conditions are seldom recorded as the location where the measurement is needed rarely coincides with the geographically fixed coarse-scale measurement pixels in the raw MC ratio raster data (Robert Brakenridge et al., 2012). To address this deficiency, Revilla-Romero et al. (2014) proposed the use of spatially averaged MC ratio values over the nearest grid cell to a measurement site of interest along with its three nearest neighbors on the original grid. While this modification was noted to increase the accuracy of the product, the resulting retrievals still exhibit considerable uncertainty, making them difficult for use in operational settings.

This study uses hydrological knowhow to propose a new method to adequately extract signals sensitive to the basin discharge from the raw MC ratio. It is demonstrated that the proposed approach offers significant improvements over the existing approach of taking the raw MC ratio at a station or an average of those over neighboring grids around the point of interest.. For the proposed approach, we first argue that the best representation of discharge across the spatial domain will coincide with the river network where flow accumulation and inundation occur. Then, it is presumed that the pixels along the river network that exhibit the greatest sensitivity to brightness temperature will be the ones exhibiting the highest water extent variations compared to upper reaches of the stream network. Based on this hypothesis, a simple method was developed in this study for enhancing the MC ratio using the well-known Topographic Wetness Index (TWI; Beven & Kirkby, 1979) as a qualitative indicator for the possibility of inundation over the terrain. The developed method was evaluated across 179 stations distributed over Australia against corresponding ground discharge measurements over a 5-year study period from 1 January 2010 to 31 December 2014. These locations are free from anthropogenic effects and represent a wide range of sizes, climates, and topographical attributes, allowing a fair assessment of how the proposed method may perform elsewhere.

This rest of the paper is organized as follows. The study area and data used in this study are presented in section 2. Details of the method are described in section 3, and then the evaluation results are shown and discussed along with future research directions in section 4. Section 5 concludes this study with a summary of the main findings reached.

2. Study and Data

2.1. Study Area

Hydrologic Reference Stations (HRS) represent a collection of high-quality monitoring locations across Australia that were identified to be free from any anthropogenic influences on resulting flows. The HRS network spans from (10–45°S, 110–155°E), and currently consists of 222 high-quality monitoring sites. For inclusion into the network, each site has at least 30 years of high-quality streamflow records with minimal regulation, land use change, and other factors (e.g., dams and irrigation), representing all hydro-climatic regions across Australia (Turner et al., 2012).

In this study, only sites for which the watershed area is more than the 0.09° × 0.09° (approximately 9 km × 9 km near the equator) grid cell size of the MC ratio product were included. As a result, 179 stations from the whole HRS network were used for evaluation purposes, and are distributed over three dominant climate zones, tropical, arid, and temperate (Peel et al., 2007), as presented in Figure 1a. The areas of these catchments range from 101 to 232,846 km^2 and elevation, 284 to 1,351 m (above sea level), as shown in Figures 1b and 1c, respectively (Ajami et al., 2017). Note that eight stations for which areas are bigger than 10,000 km^2 were not included in Figure 1b for better visualization. The discharge data for the 179 HRS stations were obtained from the Australian Bureau of Meteorology (http://www.bom.gov.au/waterdata/).

2.2. Data

2.2.1. MC Ratio

The Global Flood Detection System provides 0.09° × 0.09° gridded daily maps of the MC ratio in near real-time. The MC ratio data are based on space-borne passive microwave observations over dry and wet pixels and are available from December 1997 onward by using several passive microwave sensors over their operational periods. The original methodology behind these maps was developed by Brakenridge et al. (2007) at the Dartmouth Flood Observatory. Then, it was modified and is currently maintained by the European Commission Joint Research Centre on an automated operational basis (Kugler & De Groeve, 2007). A summary of the method used is presented here with additional details available in Brakenridge et al. (2007) and Kugler and De Groeve (2007).

The MC ratio is defined as the ratio of the brightness temperature at a frequency of 36.5 GHz (Ka band) and the H-polarization over a wet measurement pixel (T^M_{bH}) with the 95th percentile value of brightness temperature measurements over 7 × 7 neighboring calibration pixels that are regarded as dry (T^C_{bH})). This is written as

$$\text{MC ratio} = T^M_{bH}/T^C_{bH} \tag{1}$$

An increased water extent over a region generally causes a decrease in the numerator (T^M_{bH}) in equation (1)

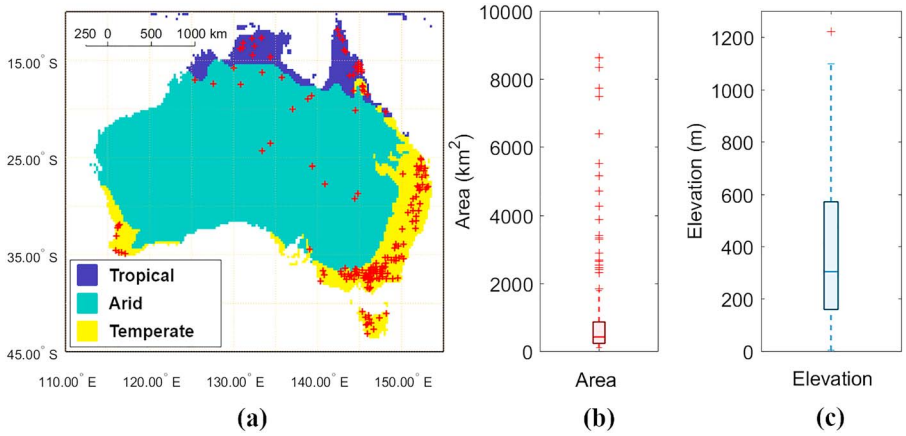

Figure 1. (a) Locations (red crosses), (b) area, and (c) elevation distributions for the 179 Hydrologic Reference Stations used in this study. The background in (a) presents three dominant climate zones, tropical, arid, and temperate, as per the updated Koppen-Geiger climate classification (Peel et al., 2007).

due to the different thermal inertia and emission properties of land and water, and accordingly, the MC ratio is reduced (De Groeve, 2010).

The MC ratio data sets are classified by the sensors used and the sampling periods adopted. Among the various sensor-derived products, the merged 4-day average product has no gaps by allowing temporal smoothening and filtering, and is well correlated with discharge data and shows promise for calibrating distributed hydrologic models compared to in situ discharge data (Revilla-Romero et al., 2015). For this reason, the merged 4-day average product over the 5-year study period was used in the results reported later.

It is worth noting that the MC ratio performs best at capturing high-flow peaks but not low flows in terms of the temporal correlation. Accordingly, the investigation reported here measures the optimality of extracted signals using the Pearson correlation (R) between the discharge values greater than the second quantile (i.e., median) of the whole series and its corresponding MC ratio at each station. Lastly, inversed values of the raw MC ratio data (i.e., T_{bH}^{C}/T_{bH}^{M}) were consistently used in this study for representing positive correlations because the raw data are negatively correlated with flood extents.

2.2.2. TWI

Existing applications of the MC ratio do not use the hydrological knowhow developed over the past that has allowed flow discharge to be related to topographically derived catchment indicators. In this study, the Topographic Wetness Index (TWI; Beven & Kirkby, 1979) is used as a comprehensive measure of flow accumulation, direction, and slope over the terrain. The TWI is a topographic index developed for representing soil moisture distribution within the rainfall-runoff model called TOPMODEL. TWI and TOPMODEL have been widely used for hydrological, ecological environmental applications (Grabs et al., 2009; Kopecký & Čížková, 2010; Pei et al., 2010; Pourali et al., 2016; Sørensen et al., 2006). Especially, TWI has been shown to exhibit strong correlations with surface water extents (i.e., floodplains) and has also been used for detecting flood-prone areas (De Risi et al., 2018; Manfreda et al., 2011). TWI is defined as

$$\mathrm{TWI} = \ln(a/\tan\beta) \tag{2}$$

where "a" is the upslope contributing area per unit contour length of a certain point through which water drainage passes and tanβ is the local slope.

Given the potential TWI offers for locating coarse-scale pixels with significant water surface extents, it was used here as the basis for refining the MC ratio. Use of TWI here helps account for hydrologically relevant topographic attributes as a quantitative indicator defining floodplains and mountainous areas. To provide context to our choice of TWI here, it was found that the correlation between the time series of discharge and MC ratio at the 179 stations varies monotonically with station TWI values, with the correlations being greater when TWI is high. The statistically significant relationship between these two suggests that the TWI at the pixel location modulates the quality of the MC ratio signal that is derived.

The TWI is usually derived from digital elevation models (DEMs). In this study, the 500-m DEM product derived from the 90-m Shuttle Radar Topographic Mission (Jarvis et al., 2008) was used, and then the method proposed by Wang and Liu (2006) was applied to the DEM to fill surface depressions using a module of the System for Automated Geoscientific Analyses–Geographic Information System (http://saga-gis.org; Conrad et al., 2015). The MATLAB-based TopoToolbox (https://topotoolbox.wordpress.com/; Schwanghart & Scherler, 2014) was used to calculate gradient (i.e., tanβ), flow direction by the steepest descent method (O'Callaghan & Mark, 1984), and flow accumulation area (i.e., a) at each grid. Finally, the TWI at 500-m spatial resolution was resampled to the spatial resolution of the MC ratio product (0.09°) by spatially averaging TWI values in each 0.09° grid cell for further assessment. In addition to this, 250-m and 1-km DEM were also used for the extraction and results compared to assess the sensitivity of DEM resolution to the flood magnitudes derived.

3. Method

Given spatially varying measurements of the MC ratio for a region, the aim of the proposed approach is to extract optimal signals at a measurement point by identifying locations having the greatest correlation R between the MC ratio and observed discharge time series. To identify these locations, two assumptions are made. First, the local area is assumed to be impacted by similar climatological forcing as other locations, and therefore exhibits similar temporal correlations against the climatological forcing. Second, the water extent affecting the MC ratio is assumed to exhibit greater sensitively in floodplains than mountainous area within the local boundary. Accordingly, the proposed method consists of two components, quantification of proximity, and extraction of optimal signals using TWI as the indicator of lowness and flatness, which are described as follows through subpanels in Figure 2.

3.1. Determination of Local Boundary for MC Ratio

The first step in the proposed method entails specifying a local domain within which optimal MC ratio signals can be identified. This domain was selected based on the spatial correlation within the MC ratio grid, as depicted in Figures 2a and 2b. An exponential model was used to represent the "correlogram" or a distance-correlation relationship (Bohling, 2005). For this, spatial Pearson correlation coefficients (C) were first calculated using all pairs of the MC ratio time series within an arbitrary boundary of 21 × 21–0.09° pixels as a function of intercell distance (D), resulting in 97,020 pairs for each panel of interest. Then the correlation estimates within 9-km bins were arithmetically averaged by considering the 0.09° grid size, and the C-D relationship fitted to the exponential model as

$$C(D) = e^{-D/r} \tag{3}$$

where r is a fitting parameter, called *range*, in the exponential model, allowing specification of a distance beyond which the estimated correlation is close to zero. A histogram of the r estimates over the 179 HRSs is presented in Figures 2a and 2b. Most of the HRSs have a range less than 60 km as shown in Figure 2a; as a result, the local boundary for each HRS was determined as 13 × 13 0.09° pixels corresponding to a radius of approximately 60 km (Figure 2b).

3.2. Extraction of MC Ratio Signal

Consider the example in Figures 2c–2g (see below for details of the three classes representing waterbody, land, and waterside) for Happy Valley Creek at Rosewhite (ID: 403214). This panel has been chosen to illustrate the sensitivity of the proposed method to lakes (Figure 2d with the circle marked B representing Lake Huma), TWI (scaled to lie between 0 and 1; Figure 2f), and the coefficient of variation (CV) of the MC ratio at each pixel (Figure 2g). The CV at each pixel is calculated by dividing the standard deviation of the MC ratio time series (S) with its mean (M; i.e., CV = S/M). The center of Figures 2d–2g is the discharge measurement location (marked X). Figure 2e shows the correlation between the discharge (at X) and the MC ratio time series at each pixel.

As presented in Figures 2c–2g, the following characteristics of MC ratio were generally identified across all HRSs with relation to the local topography and its impact on the measured discharge values. First, most importantly, the best MC ratio signal tends not to lie at the center where the discharge measuring station exists (Figure 2e). Rather, much like the area marked "A" in Figure 2d, a good correlation appears on

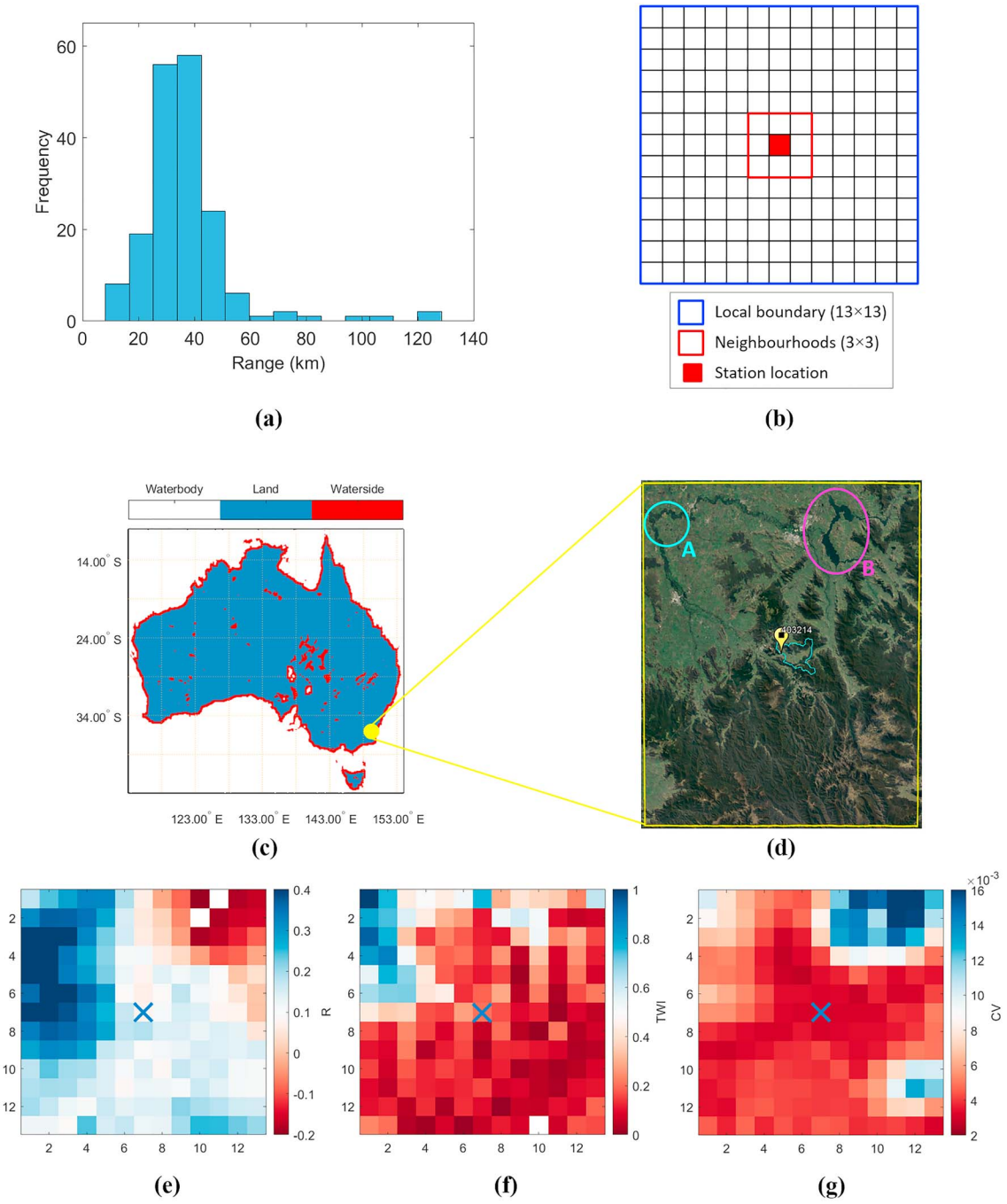

Figure 2. (a) Histogram presenting the distribution of ranges over the 179 HRSs. (b) Determined local boundary consisting of 13 × 13 0.09° pixels over which an HRS is centered. (c) Map representing the distribution of the three classes adopted in this study, waterbody, land, and waterside, along with an illustrative study location, Happy Valley Creek at Rosewhite station (ID: 403214). (d) Satellite image, catchment boundary, with the area marked "A" showing highest correlation between the MC ratio and the station discharge. Also note Lake Huma (marked "B") representing a region with artificially high MC ratios that need masking. (e) Correlation coefficients (*R*) between the station (marked "X") discharge and the MC ratio, (f) the distribution of TWI values scaled 0 to 1, and (g) the coefficients of variation of the MC ratio over all pixels. HRS = Hydrologic Reference Station; MC = Measurement-Calibration.

pixels at which the TWI is relatively high within the local boundary even though these pixels may lie out of the catchment boundary (Figure 2f). Second, low correlation coefficients were generally noted over regions with a highly fluctuating water extent represented by high CV values, which usually represent a waterside (as described in section 2.2.1), or a local lake (marked "B" in Figure 2d).

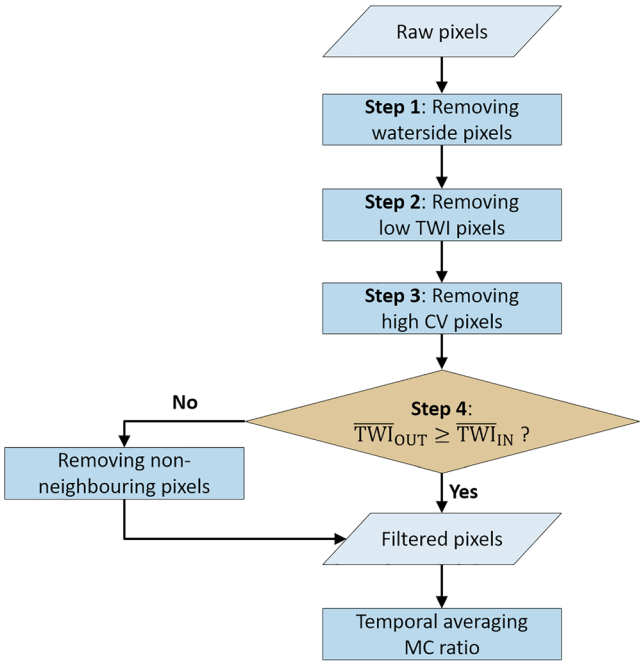

Figure 3. Flow chart for extracting MC ratio signal through sequential image segmentation of TWI and CV within the local boundary. MC = Measurement-Calibration; TWI = Topographic Wetness Index; CV = coefficient of variation.

Given these observations, it is hypothesized that the optimal signal can be extracted after removing unsuitable pixels represented by low TWIs and high CVs to remove both mountainous and high fluctuation regions. For this process, our proposed procedure for extracting MC ratio uses four major steps as presented in Figure 3.

Steps 1 to 3 are implemented using the gray image thresholding method originally developed by Otsu (1979) and modified by Xue and Titterington (2011). This method allows robust identification of pixels exceeding a defined threshold in gray images within which pixel-level distributions are highly skewed or heavy-tailed. A summary of the thresholding method is presented below with more details for interested readers in the two references cited earlier.

For an image consisting of N pixels where each pixel is represented by gray levels (i.e., x_i, $i = 1, ..., N$, where x_i represents a number between 0 and 255 with 255 representing the highest gray level possible), an unknown gray threshold t divides the image into two segments $C_1(t)$ and $C_2(t)$ such that

$$C_1(t) = \{i : 0 \leq x_i \leq t, 1 \leq i \leq N\}, \quad C_2(t) = \{i : t < x_i \leq T, 1 \leq i \leq N\} \tag{4}$$

where T is the largest gray level (255 for an 8-bit image), or, $x_i \in [0, T]$). In the context of the problem attempted here, a gray level could represent TWI or the CV of the MC ratio. To estimate the optimal threshold t_o^*, a histogram for the image, h(x), is constructed by dividing each gray level frequency by N, such that $\sum_{x=0}^{T} h(x) = 1$. Otsu (1979) presented an objective function to find the optimal threshold t_o^* as

$$t_o^* = \arg\min_t \{w_1(t)s_1^2(t) + w_2(t)s_2^2(t)\} \tag{5}$$

where $w_1(t)$ and $w_2(t)$ denote proportions of pixels representing the segments $C_1(t)$ and $C_2(t)$ separated by a threshold t, and $s_1(t)$ and $s_2(t)$ are the sample standard deviations for the two segments of the image, which are defined as

$$w_1(t) = \sum_{x=0}^{t} h(x), \quad w_2(t) = \sum_{x=t+1}^{T} h(x) = 1 - w_1(t) \tag{6}$$

$$s_1(t) = \sum_{x=0}^{t} \left\{ \frac{h(x)}{w_1(t)} (x - \overline{x_1}(t))^2 \right\}, \quad s_2(t) = \sum_{x=t+1}^{T} \left\{ \frac{h(x)}{w_2(t)} (x - \overline{x_2}(t))^2 \right\} \tag{7}$$

where $\overline{x_1}(t)$ and $\overline{x_2}(t)$ are the sample mean values for $C_1(t)$ and $C_2(t)$, respectively.

For this, Xue and Titterington (2011) suggested using mean absolute deviations from the medians instead of $s_1(t)$ and $s_2(t)$ to be more robust to skewed or heavy-tailed distributions of $C_1(t)$ and $C_2(t)$. Namely,

$$g_o^* = \arg\min_t \{w_1(t)MAD_1(t) + w_2(t)MAD_2(t)\} \tag{8}$$

where $MAD_1(t)$ and $MAD_2(t)$ are the mean absolute deviations from the medians (i.e., $m_1(t)$ and $m_2(t)$) for $C_1(t)$ and $C_2(t)$, respectively, and are calculated as

$$MAD_1(t) = \sum_{x=0}^{t} \left\{ \frac{h(x)}{w_1(t)} |x - m_1(t)| \right\}, \quad MAD_2(t) = \sum_{x=t+1}^{T} \left\{ \frac{h(x)}{w_2(t)} |x - m_2(t)| \right\} \tag{9}$$

In this study, equation (8) has been consistently used for steps 1 to 3 in Figure 3. For step 1, grids on and contiguous to open water bodies (e.g., the sea or lakes) were excluded from the analysis to avoid water surface fluctuations effects. For this, the coefficients of variation (CV) of the MC ratio time series were first calculated for all pixels and then the median-based image thresholding method was applied for automatically segmenting high CV pixels that are regarded as waterside in this study. Then, three lines of pixels

(approximately 25 km) along the waterbodies were additionally masked consistent with what has been commonly used for applications using coarse-scale passive microwave-derived land surface products (Kim, Liu, et al., 2015; Kim, Parinussa, et al., 2015). Consequently, as depicted in Figure 2c, the study area was classified into three classes, waterbody, land, and waterside, and then the classes of waterbody and waterside were excluded from further analyses. In the same way, low-TWI and high-CV pixels were sequentially removed through steps 2 and 3. Finally, in step 4, the mean TWI values for remaining pixels within the 3 × 3 neighborhood area (Figure 2b) when equal to or larger than the mean for nonneighboring pixels, resulted in the nonneighboring pixels being additionally removed from further consideration. This ensured that the assessment was restricted to pixels that broadly represent the river network and not the mountainous areas where possibly high MC ratio measurements would be spurious.

For the filtered pixels through steps 1 to 4, the arithmetically averaged MC ratio, for a n-day period over which the assessment is performed, can be expressed as

$$\mathbf{MC}_{\text{ext}} = \frac{\sum_{i \in a_p} \mathbf{MC}_i}{P} \tag{10}$$

where $\mathbf{MC}_{\text{ext}}$ is the extracted MC ratio signal from the local boundary as a vector of size $n \times 1$, a_p is the partial area over the local boundary which remains after the removal of unsuitable pixels, i is the spatial index for a pixel over a_p where the MC ratio ($\mathbf{MC}_i$) exists, and P is the total number of pixels considered.

4. Results and Discussion

Figure 4 illustrates the sequential procedure described in section 3.2 using the Happy Valley Creek at Rosewhite station (ID: 403214) as an example. In this example, the proposed approach using a 500-m DEM is referred to as $\text{TWI}_{500\text{m}}$. In addition, "Center" denotes the case where the MC ratio at the station location is used, and "3NEI" denotes when a spatial average of MC ratio at the nearest grid cell to the station and its three nearest neighbors as used as proposed by Revilla-Romero et al. (2014) is used.

The raw pixels (Figure 4a) are sequentially filtered through steps 2 and 3 (Figures 4b and 4c). Then vectors of MC ratio signals over the remaining pixels are arithmetically averaged by equation (10). An example of how the proposed signal extraction method works is presented in Figure 4d, showing time series plots of observed flows and extracted MC ratios during the 5-year study period. While the proposed approach ($\text{TWI}_{500\text{ m}}$) presents a moderate temporal correspondence with observations ($R = 0.410$), the 3NEI approach shows a weak correlation ($R = 0.088$) for which observations clearly exhibit the seasonality present in the data.

The box plots showing overall R values from the various MC ratio extraction approaches for all 179 HRSs in Figure 4e clearly show the improvement the proposed approach exhibits in relation to the alternatives (Center and 3NEI) currently in use. Here while the Manual approach indicates the best MC ratio providing the maximum R with observed discharge within the local boundary, it is not possible to use it without ground discharge data. It should be noted that the Center and 3NEI alternatives provided almost identical results and were significantly inferior to the Manual case. This result confirms the need for a better approach for estimating MC ratio than what is currently in use. As Figure 4e illustrates, the proposed approaches using the various sizes of DEMs show little sensitivity to resolution and show significantly better results than the Center or 3NEI alternatives. In general, in case of $\text{TWI}_{500\text{ m}}$, 144 out of 179 HRSs (80%) showed significantly larger R values (0.292 ± 0.153) than those from the Center and 3NEI approaches (0.132 ± 0.160 and 0.130 ± 0.166, respectively). Only 35 stations (20%) presented smaller R values than the two existing approaches. This degradation in performance generally appeared at locations where TWI distributions are relatively platykurtic, and therefore, the median-based image thresholding does not work properly by removing pixels in the 3 × 3 neighborhood area. However, the degradations were not so significant as the three sets of means for all such catchments were calculated as 0.306 ± 0.215, 0.351 ± 0.219, and 0.353 ± 0.236 for $\text{TWI}_{500\text{ m}}$, Center, and 3NEI, respectively.

While this outcome has considerable promise for generalization in ungauged catchments worldwide, there are a few research questions that need to be addressed to further refine the approach presented here. First, TWI was the only topographic index considered in this study for identifying discharge-sensitive locations and filtering out insensitive areas. However, the sensitivity of the extracted MC ratio can be assessed

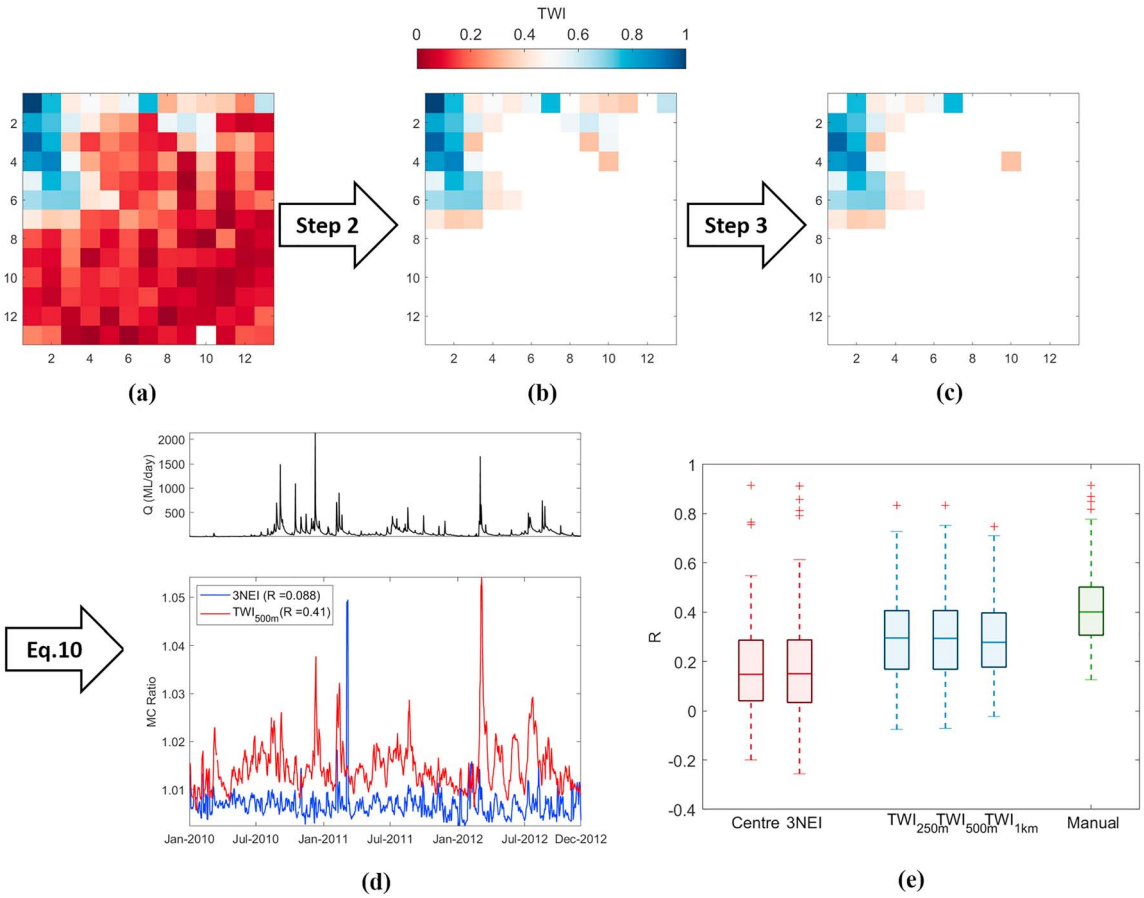

Figure 4. Illustration of MC ratio signal extraction algorithm for Happy Valley Creek at Rosewhite station (ID: 403214), where (a) shows raw pixels over the local boundary; (b) shows remaining pixels after removing low TWI pixels (step 2); (c) shows remaining pixels after removing high coefficient of variation pixels (step 3); (d) shows time series plots of observed flows (top panel), MC ratio signals extracted by 3NEI (bottom panel, blue line), and the proposed TWI-based approach using 500-m digital elevation model (bottom panel, red line) approaches, respectively; and (e) shows a box plot presenting overall *R* values over the 179 Hydrologic Reference Stations from alternate MC ratio extraction approaches considered, denoted Center, 3NEI, TWI (250 m, 500 m, and 1 km), and Manual, respectively. Note that "Manual" here represents a manual search of the highest correlation MC ratio pixel, not possible unless discharge measurements are available and the whisker length of the box plots corresponds to approximately $\pm 2.7\sigma$ and 99.3% coverage if the data are normally distributed. TWI = Topographic Wetness Index; MC = Measurement-Calibration.

using different indices such as Multi-resolution Valley Bottom Flatness Index, plan curvature, or some combination thereof, instead of resorting to TWI alone. In addition, potential errors in the calculation of topographic indices using larger-grid DEMs should be carefully considered (Quinn et al., 1995). Second, identification of a MC ratio pixel outside the catchment domain implies the presence of storm systems that impact high flows in neighboring catchments. This assumption may not be appropriate in certain types of climates and needs to be assessed on a case-by-case basis. Third, extending the evaluation to other regions under different conditions would be valuable to verify that the proposed method is generically applicable and not specific to Australian conditions which offer unique differences (such as little snow impact) than other parts of the world.

5. Conclusions

In this study, a simple approach has been proposed for automatically extracting signals sensitive to the basin discharge from a passive microwave-derived data, the MC ratio, using a topographic index, TWI as an indicator defining floodplains, and mountainous area using coarse-scale digital elevation data. As the MC ratio performs well at capturing high discharges but not low values, it was assessed at each station using the Pearson correlation between discharge greater than the median discharge with its corresponding MC ratio.

The simplicity of the approach presented lies in using only the DEM-derived TWI, under the assumption that satellite readings will be more sensitive to changes in water extents in floodplains which have higher TWI values. To account for this, the proposed method weights MC ratio retrievals in proportion to the TWI values within a local boundary exhibiting similar climatology. Then, an arithmetic average of resulting values is formed and considered as a proxy for the observed discharge values.

TWI has been used to extract the MC ratio from 179 Hydrologic Reference Stations (HRS) over Australia representing various climatic conditions, watershed sizes, and elevations. The results here were directly compared with existing methods that simply take the MC ratio at the gauging station and/or neighboring pixels and provided a markedly improved representation of the observed discharge. Therefore, it is expected that the proposed method can expand the applicability of the MC ratio data over ungauged basins (Kim et al., 2018), creating new opportunities for hydrologic model specification (Tang et al., 2018) and design flood or environmental flow estimation.

Acknowledgments
This work has been undertaken as part of a project funded by the Australian Research Council, WaterNSW, and Sydney Water. We are grateful to all contributors to the data sets used in this study. Particularly, we thank the teams from the Bureau of Meteorology (BoM) Australia and the Global Flood Detection System. The data sets can be freely obtained as follows. The discharge data and related information of the Hydrologic Reference Stations from the BoM Australia (http://www.bom.gov.au/water/hrs/index.shtml), the MC ratio data from the GFDS (http://www.gdacs.org/flooddetection/), and the DEM data from Shuttle Radar Topographic Mission (SRTM; http://www.cgiar-csi.org/).

References

Ajami, H., Sharma, A., Band, L. E., Evans, J. P., Tuteja, N. K., Amirthanathan, G. E., & Bari, M. A. (2017). On the non-stationarity of hydrological response in anthropogenically unaffected catchments: An Australian perspective. *Hydrology and Earth System Sciences*, *21*(1), 281–294. https://doi.org/10.5194/hess-21-281-2017

Beven, K. J., & Kirkby, M. J. (1979). A physically based, variable contributing area model of basin hydrology/Un modèle à base physique de zone d'appel variable de l'hydrologie du bassin versant. *Hydrological Sciences Bulletin*, *24*(1), 43–69. https://doi.org/10.1080/02626667909491834

Bohling, G. (2005). Introduction to geostatistics and variogram analysis. *Kansas Geological Survey*, 1–20.

Brakenridge, G. R., Nghiem, S. V., Anderson, E., & Mic, R. (2007). Orbital microwave measurement of river discharge and ice status. *Water Resources Research*, *43*, W04405. https://doi.org/10.1029/2006WR005238

Calmant, S., & Seyler, F. (2006). Continental surface waters from satellite altimetry. *Comptes Rendus Geoscience*, *338*(14-15), 1113–1122. https://doi.org/10.1016/j.crte.2006.05.012

Conrad, O., Bechtel, B., Bock, M., Dietrich, H., Fischer, E., Gerlitz, L., et al. (2015). System for Automated Geoscientific Analyses (SAGA) v.2.1.4. *Geoscientific Model Development*, *8*(7), 1991–2007. https://doi.org/10.5194/gmd-8-1991-2015

De Groeve, T. (2010). Flood monitoring and mapping using passive microwave remote sensing in Namibia. *Geomatics, Natural Hazards and Risk*, *1*(1), 19–35. https://doi.org/10.1080/19475701003648085

De Risi, R., Jalayer, F., De Paola, F., & Lindley, S. (2018). Delineation of flooding risk hotspots based on digital elevation model, calculated and historical flooding extents: The case of Ouagadougou. *Stochastic Environmental Research and Risk Assessment*, *32*(6), 1545–1559. https://doi.org/10.1007/s00477-017-1450-8

Fekete, B. M., & Vörösmarty, C. J. (2002). The current status of global river discharge monitoring and potential new technologies complementing traditional discharge measurements. Paper presented at the Predictions in Ungauged Basins: PUB kick-off (Proceedings of the PUB kick-off meeting held in Brasilia, 20–22 November 2002). IAHS Publication.

Grabs, T., Seibert, J., Bishop, K., & Laudon, H. (2009). Modeling spatial patterns of saturated areas: A comparison of the topographic wetness index and a dynamic distributed model. *Journal of Hydrology*, *373*(1–2), 15–23. https://doi.org/10.1016/j.jhydrol.2009.03.031

GRDC/BfG (2018). Station maps—Spatial distribution of GRDC stations indicated by time series end or length. Retrieved from http://www.bafg.de/GRDC/EN/02_srvcs/21_tmsrs/stationMaps.html?nn=201566

Hou, J., van Dijk, A. I., Renzullo, L. J., & Vertessy, R. A. (2018). Using modelled discharge to develop satellite-based river gauging: a case study for the Amazon Basin. *Hydrology and Earth System Sciences*, *22*(12), 6435–6448.

Jarvis, A., Reuter, H. I., Nelson, A., & Guevara, E. (2008). Hole-filled seamless SRTM data V4, International Centre for Tropical Agriculture (CIAT). In.

Khan, S. I., Hong, Y., Vergara, H. J., Gourley, J. J., Brakenridge, G. R., Groeve, T. D., et al. (2012). Microwave satellite data for hydrologic modeling in ungauged basins. *IEEE Geoscience and Remote Sensing Letters*, *9*(4), 663–667. https://doi.org/10.1109/LGRS.2011.2177807

Kim, S., Liu, Y. Y., Johnson, F. M., Parinussa, R. M., & Sharma, A. (2015). A global comparison of alternate AMSR2 soil moisture products: Why do they differ? *Remote Sensing of Environment*, *161*(0), 43–62. https://doi.org/10.1016/j.rse.2015.02.002

Kim, S., Paik, K., Johnson, F. M., & Sharma, A. (2018). Building a flood-warning framework for ungauged locations using low resolution, open-access remotely sensed surface soil moisture, precipitation, soil, and topographic information. *IEEE Journal of Selected Topics in Applied Earth Observations and Remote Sensing*, *11*(2), 375–387. https://doi.org/10.1109/JSTARS.2018.2790409

Kim, S., Parinussa, R. M., Liu, Y. Y., Johnson, F. M., & Sharma, A. (2015). A framework for combining multiple soil moisture retrievals based on maximizing temporal correlation. *Geophysical Research Letters*, *42*, 6662–6670. https://doi.org/10.1002/2015gl064981

Kopecký, M., & Čížková, Š. (2010). Using topographic wetness index in vegetation ecology: Does the algorithm matter? *Applied Vegetation Science*, *13*(4), 450–459. https://doi.org/10.1111/j.1654-109X.2010.01083.x

Kugler, Z., & De Groeve, T. (2007). The Global Flood Detection System. Retrieved from Luxembourg: Office for Official Publications of the European Communities:

Manfreda, S., Leo, M. D., & Sole, A. (2011). Detection of flood-prone areas using digital elevation models. *Journal of Hydrologic Engineering*, *16*(10), 781–790. https://doi.org/10.1061/(ASCE)HE.1943-5584.0000367

O'Callaghan, J. F., & Mark, D. M. (1984). The extraction of drainage networks from digital elevation data. *Computer Vision, Graphics, and Image Processing*, *28*(3), 323–344. https://doi.org/10.1016/S0734-189X(84)80011-0

Otsu, N. (1979). A threshold selection method from gray-level histograms. *IEEE Transactions on Systems, Man, and Cybernetics*, *9*(1), 62–66. https://doi.org/10.1109/TSMC.1979.4310076

Peel, M. C., Finlayson, B. L., & McMahon, T. A. (2007). Updated world map of the Köppen-Geiger climate classification. *Hydrology and Earth System Sciences*, *11*(5), 1633–1644. https://doi.org/10.5194/hess-11-1633-2007

Pei, T., Qin, C. Z., Zhu, A. X., Yang, L., Luo, M., Li, B. L., & Zhou, C. H. (2010). Mapping soil organic matter using the topographic wetness index: A comparative study based on different flow-direction algorithms and kriging methods. *Ecological Indicators*, *10*(3), 610–619. https://doi.org/10.1016/j.ecolind.2009.10.005

Pourali, S. H., Arrowsmith, C., Chrisman, N., Matkan, A. A., & Mitchell, D. (2016). Topography wetness index application in flood-risk-based land use planning. *Applied Spatial Analysis and Policy*, *9*(1), 39–54. https://doi.org/10.1007/s12061-014-9130-2

Quinn, P., Beven, K., & Lamb, R. (1995). The in (a/tan/β) index: How to calculate it and how to use it within the topmodel framework. *Hydrological Processes*, *9*(2), 161–182. https://doi.org/10.1002/hyp.3360090204

Revilla-Romero, B., Beck, H. E., Burek, P., Salamon, P., de Roo, A., & Thielen, J. (2015). Filling the gaps: Calibrating a rainfall-runoff model using satellite-derived surface water extent. *Remote Sensing of Environment*, *171*, 118–131. https://doi.org/10.1016/j.rse.2015.10.022

Revilla-Romero, B., Thielen, J., Salamon, P., De Groeve, T., & Brakenridge, G. R. (2014). Evaluation of the satellite-based global flood detection system for measuring river discharge: Influence of local factors. *Hydrology and Earth System Sciences*, *18*(11), 4467–4484. https://doi.org/10.5194/hess-18-4467-2014

Robert Brakenridge, G., Cohen, S., Kettner, A. J., De Groeve, T., Nghiem, S. V., Syvitski, J. P. M., & Fekete, B. M. (2012). Calibration of satellite measurements of river discharge using a global hydrology model. *Journal of Hydrology*, *475*(0), 123–136. https://doi.org/10.1016/j.jhydrol.2012.09.035

Schwanghart, W., & Scherler, D. (2014). Short communication: TopoToolbox 2-MATLAB-based software for topographic analysis and modeling in Earth surface sciences. *Earth Surface Dynamics*, *2*(1), 1–7. https://doi.org/10.5194/esurf-2-1-2014

Sørensen, R., Zinko, U., & Seibert, J. (2006). On the calculation of the topographic wetness index: Evaluation of different methods based on field observations. *Hydrology and Earth System Sciences*, *10*(1), 101–112. https://doi.org/10.5194/hess-10-101-2006

Tang, Y., Marshall, L., Sharma, A., & Ajami, H. (2018). A Bayesian alternative for multi-objective ecohydrological model specification. *Journal of Hydrology*, *556*, 25–38. https://doi.org/10.1016/j.jhydrol.2017.07.040

Tarpanelli, A., Brocca, L., Lacava, T., Melone, F., Moramarco, T., Faruolo, M., et al. (2013). Toward the estimation of river discharge variations using MODIS data in ungauged basins. *Remote Sensing of Environment*, *136*, 47–55. https://doi.org/10.1016/j.rse.2013.04.010

Turner, M., Bari, M., Amirthanathan, G., & Ahmad, Z (2012). Australian network of hydrologic reference stations-advances in design, development and implementation. Paper Presented at the Hydrology and Water Resources Symposium 2012, Sydney, Australia.

Van Dijk, A. I., Brakenridge, G. R., Kettner, A. J., Beck, H. E., De Groeve, T., & Schellekens, J. (2016). River gauging at global scale using optical and passive microwave remote sensing. *Water Resources Research*, *52*, 6404–6418. https://doi.org/10.1002/2015WR018545

Wang, L., & Liu, H. (2006). An efficient method for identifying and filling surface depressions in digital elevation models for hydrologic analysis and modelling. *International Journal of Geographical Information Science*, *20*(2), 193–213. https://doi.org/10.1080/13658810500433453

Xue, J.-H., & Titterington, D. M. (2011). Median-based image thresholding. *Image and Vision Computing*, *29*(9), 631–637. https://doi.org/10.1016/j.imavis.2011.06.003